All-fiber three-path Mach–Zehnder interferometer

Gregor Weihs, Michael Reck, Harald Weinfurter, and Anton Zeilinger

Institut für Experimentalphysik, Universität Innsbruck, Technikerstrasse 25, A-6020 Innsbruck, Austria

Received August 14, 1995

We report the realization of a three-path Mach–Zehnder interferometer using single-mode fibers and two integrated 3×3 fiber couplers. We observed enhanced phase sensitivity, as compared with two-path interferometers, with a visibility of the interference pattern of more than 97%. This interferometer has an analog in two-photon interferometry, and we believe it to be the first nontrivial example of $N \times N$ multiport interferometers. © 1996 Optical Society of America

Multipath interferometers permit optical realizations of discrete unitary operators in higher-dimensional Hilbert spaces[1] in tests of the foundations of quantum mechanics. All fiber quantum cryptography and Bell-inequality experiments have been realized with two-path inteferometers.[2] Here we present a multipath interferometric experiment, using single-mode fiber technology.

Although conventional two-path interferometers are being steadily improved by various techniques, there have been nearly no efforts to exploit the enhanced sensitivity of many-path interferometers.[3,4] One of the main reasons is that setting up such a device with discrete optical components is a formidable task. However, single-mode optical fiber technology provides an easy way to set up complex interferometers with standard commercial $N \times N$ couplers. In this Letter we demonstrate the basic operational principles of such $N \times N$ fiber-coupler interferometers for the case $N = 3$. These fiber interferometers can provide insights into multipath interferometry that later may be exploited in integrated optical devices.

Figure 1 shows a schematic of a general N-path interferometer consisting of two $N \times N$ beam splitters (multiports). Each multiport is described by an $N \times N$ matrix, which is unitary for a lossless device. In our experiment the multiports were commercially available symmetric 3×3 fiber couplers (tritters).

A symmetric device is described by a unimodular matrix. A standard form of the tritter matrix T, in which the first column and first row are real, is given by[5]

$$T = \frac{1}{\sqrt{3}} \begin{bmatrix} 1 & 1 & 1 \\ 1 & \exp\left(i\frac{2\pi}{3}\right) & \exp\left(i\frac{4\pi}{3}\right) \\ 1 & \exp\left(i\frac{4\pi}{3}\right) & \exp\left(i\frac{2\pi}{3}\right) \end{bmatrix}. \quad (1)$$

The operation of the whole setup on the input modes is then described by the system matrix M, which is the product of two tritter matrices T and a phase matrix P:

$$M = TPT = T \begin{bmatrix} \exp(i\phi_1) & 0 & 0 \\ 0 & \exp(i\phi_2) & 0 \\ 0 & 0 & \exp(i\phi_3) \end{bmatrix} T. \quad (2)$$

In our experiment light is incident on only one input (see Fig. 2) and is linearly polarized. We therefore restrict our analysis to waves of identical polarization, for which a scalar-wave analysis is sufficient. The input field $\mathbf{K}^{\text{in}} = (E^{\text{in}}, 0, 0)$ is a vector whose elements are the amplitudes of the input modes to the interferometer. $\mathbf{K}^{\text{in}}$ is transformed by the interferometer into an output vector $(E_1^{\text{out}}, E_2^{\text{out}}, E_3^{\text{out}}) = M\mathbf{K}^{\text{in}}$. We measure the intensities I_n $(n = 1, 2, 3)$ at the three outputs:

$$I_n = |E_n^{\text{out}}|^2 = I_0/9[3 + 2\cos(\phi_1 - \phi_2 + \theta_n) + 2\cos(\phi_2 - \phi_3 + \theta_n) + 2\cos(\phi_3 - \phi_1 + \theta_n)], \quad (3)$$

where $I_0 = |E^{\text{in}}|^2$ is the input intensity and the phase shifts between the outputs are given by $(\theta_1, \theta_2, \theta_3) = (0, -2\pi/3, 2\pi/3)$. The output intensity depends only on phase differences, which we write as $\varphi = \phi_1 - \phi_2$ and $\chi = \phi_2 - \phi_3$.

Note that it can be shown that identical equations have been derived for proposed experiments, in which correlated photons from a downconversion source are fed into two separate tritters and the outputs are detected in coincidence.[6] Such setups provide demonstrations of Einstein–Podolsky–Rosen correlations and tests of Bell's inequalities in higher-dimensional Hilbert spaces.

Equation (3) describes an ideal lossless interferometer. When accounting for losses present in any real experiment, we need only consider those occurring between the two tritters because all external losses are equivalent to a reduction of detection efficiency and/or source strength. The internal losses and the phases

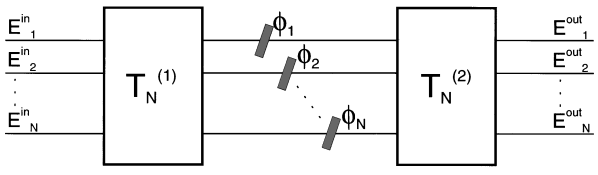

Fig. 1. Schematic of an N-path interferometer. $(E_1^{\text{in}}, E_2^{\text{in}}, \ldots E_N^{\text{in}})$ are the electric-field amplitudes at the input modes of the first $N \times N$ beam splitter (multiport), and $(E_1^{\text{out}}, E_2^{\text{out}}, \ldots E_N^{\text{out}})$ are the output amplitudes of the second one. The multiports are described by the matrices $T_N^{(1)}$ and $T_N^{(2)}$. $\phi_1, \phi_2, \ldots \phi_N$ are the phases accumulated by the fields on their paths between the multiports.

0146-9592/96/040302-03$6.00/0

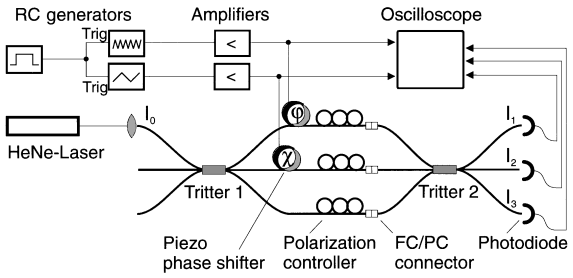

Fig. 2. Schematic of our three-path interferometer setup. The tritters are three-way integrated fiber couplers. Polarization controllers were used to adjust the polarization manually in all three arms for maximal visibility. Piezo tubes were used to modulate the interferometer phases ϕ and χ in two of the three interferometer arms. The photodiode signals and the driving signals were recorded in a digital storage oscilloscope.

φ and χ can be mathematically represented by the nonunitary phase matrix

$$P' = \begin{bmatrix} t_1 & 0 & 0 \\ 0 & t_2 \exp(i\varphi) & 0 \\ 0 & 0 & t_3 \exp(i\chi) \end{bmatrix}, \quad (4)$$

where t_1, t_2, and t_3 are the amplitude transmission factors ($0 \le t_n \le 1$) inside each arm of the interferometer. After replacement of P by P' in Eq. (2) the intensities at the three output ports are given by

$$I_n = I_0/9[{t_1}^2 + {t_2}^2 + {t_3}^2 + 2t_2 \cos(\varphi + \theta_n) + 2t_3 \cos(\chi + \theta_n) + 2t_2 t_3 \cos(\varphi - \chi + \theta_n)]. \quad (5)$$

Gray-scale plots of predicted and measured intensities are shown in Fig. 3. The section curves along the diagonal $\varphi = -\chi$ (Fig. 4) show the sidelobes that are characteristic of a three-path interferometer. In general, as with the diffraction pattern of an N-slit configuration illuminated by a plane wave, there are $N - 2$ sidelobes between the main peaks in the interference pattern of an N-path interferometer. Using the definition of the sensitivity S as the derivative of the output intensity with respect to a phase,[7]

$$S = \frac{1}{I_0} \left| \frac{dI}{d\varphi} \right|, \quad (6)$$

we see that an N-path interferometer provides higher sensitivity to phase changes than a two-path interferometer because the slopes of the main peaks are steeper.

Our interferometer (Fig. 2) was built from two single-mode fiber tritters (3×3 couplers, manufactured by SIFAM Ltd., England) with symmetric power division ratios at the operational wavelength of 633 nm. We used piezo cylinders, each wound with two loops of fiber, as phase shifters in two of the three arms. The manual polarization controller in each path consisted of three tiltable disks, each bearing two loops of fiber. Induced birefringence[8] in the coiled fiber permits any state of polarization to be reached by a proper setting of the three disks.[9] To provide easy handling of the setup, we equipped the outputs of the first tritter and the inputs of the second with fiber connectors.

Our light source was a 10-mW He–Ne laser coupled to the fiber by use of a standard M20 microscope objective. The phase shifters were driven with *RC* generators, which had a common trigger to ensure phase stability, followed by high-voltage amplifiers. To make the collected data easy to interpret, we drove the two phases at different frequencies; these were limited on the lower end (1 Hz) by the stability of our *RC* generators and on the higher end (100 Hz) by the cutoff frequency of the piezo tubes and the fiber response. The generators were therefore set to frequencies of approximately 2 and 80 Hz. The use of triangular waveforms resulted in a linear phase sweep over the whole parameter space of $[0, 2\pi] \times [0, 2\pi]$. At the outputs of the second tritter the light was detected by standard photodiodes. Their signals as well as the piezo voltages were displayed and recorded on a digital storage oscilloscope.

By tilting the disks of the three polarization controllers we adjusted the state of polarization in each arm to attain maximum visibility of the interference pattern. First, one of the two arms containing a phase shifter was disconnected, leaving only the interfer-

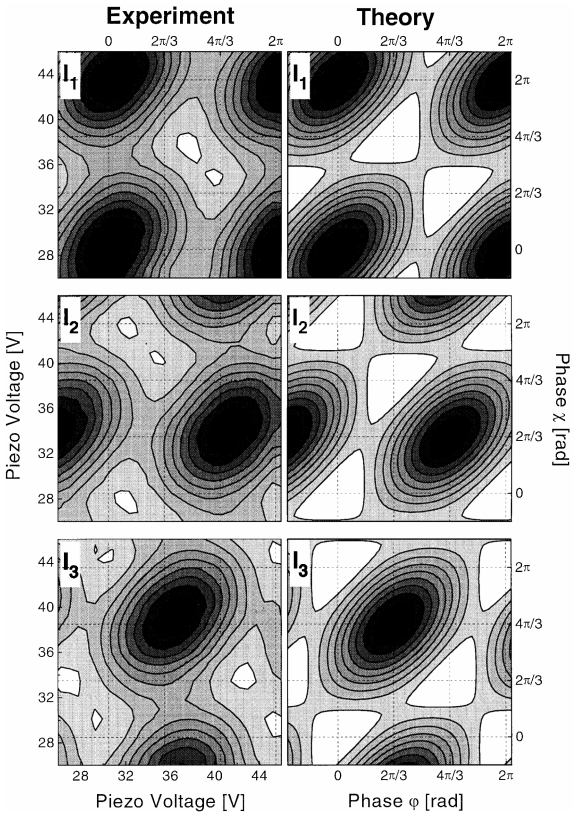

Fig. 3. Experimental data as gray-scale plots (minimum, white; maximum, black) of the measured intensities I_1–I_3 (see Fig. 2) as functions of the voltages applied to the phase shifters (left column). The corresponding theoretical functions given by Eq. (3) are shown in the right column. The phase axes were calibrated by separate measurements with one arm of the interferometer disconnected. The experimental data show only slightly reduced visibility, resulting in smaller white areas in the plot compared with the theoretical calculation.

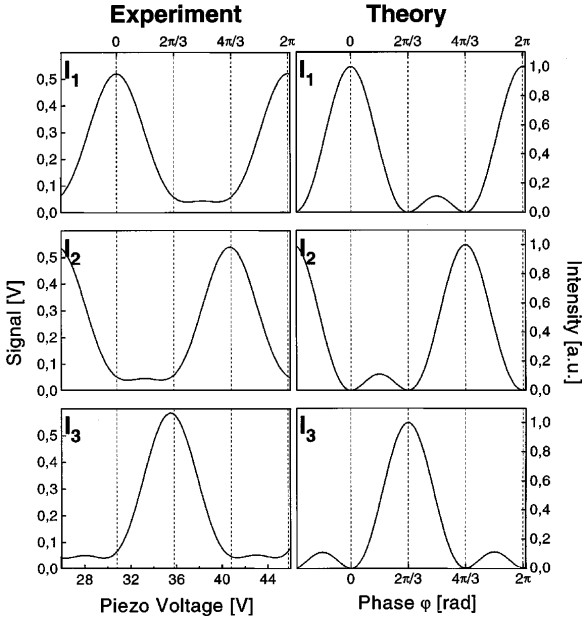

Fig. 4. Diagonal cut through the three-dimensional plots reveals the typical structure of a three-path interferometer with two peaks in each 2π phase interval. The higher phase sensitivity stems from the fact that the resulting peaks are thus steeper than the sinusoidal signal of a two-path interferometer. The diagonal phase-space cuts show a lower visibility than the total interference patterns since the absolute minima and maxima are not exactly on the diagonal line (see Fig. 3). This is due to slight differences in the transmissions of the three interferometer arms. Again, the experimental data compare well with theoretical predictions.

ence pattern of a conventional two-path interferometer. Adjusting the polarizations in the two remaining arms yielded interference visibilities of greater than 99%. The second arm containing a phase shifter was then disconnected and the formerly blocked path reactivated. After adjusting only the polarization in the latter arm we were able to achieve equally high visibilities. Finally, after reconnecting all interferometer arms and fine tuning the polarization, we attained a maximum visibility of 97% for the three-beam Mach–Zehnder interferometer.

For each measurement, we collected 5000 data points per channel. Because of the hysteresis of the piezos, we divided the data into parts corresponding to the rising and falling slopes of the triangular waveforms. All data collected at the peaks of the triangular waveforms, and hence showing nonlinear phase shifts, had to be discarded. The remaining data ($\sim$900 points per channel) were spread homogeneously over the whole phase space. Contour plots of the experimental data are shown in Fig. 3.

By using a nonlinear least-squares fit of Eq. (5) to our raw data we were able to extract the corresponding parameters I_0, t_1, t_2, and t_3 of the model. From these parameters we calculated the three section curves shown in the right column of Fig. 4. They show the characteristic sidelobes predicted by the theoretical analysis. Despite the losses in our system the relative phase sensitivity S had a maximum value of 0.60 ± 0.01 rad^{-1}, which is less than the theoretical value of 0.78 rad^{-1} but significantly more than the theoretical value of 0.50 rad^{-1} for a lossless two-path interferometer.

In summary we have realized what to our knowledge is the first all-fiber three-path Mach–Zehnder interferometer. We have shown that the output intensities satisfy the same equations as the correlations of two photons in a quantum optical experiment with two separate tritters.[6] We have further shown that a three-path interferometer displays enhanced sensitivity, which is clearly important in many applications of interferometric measurement. Further experiments in the foundations of quantum physics and the realization of higher-dimensional systems with optical fiber multiports are under way.

This study was supported by the Fonds zur Förderung der Wissenschaftlichen Forschung (Austrian Science Foundation), Schwerpunkt Quantenoptik, project S6502.

References

1. M. Reck, A. Zeilinger, H. Bernstein, and P. Bertani, Phys. Rev. Lett. **73,** 58 (1994).
2. P. D. Townsend, J. G. Rarity, and P. R. Tapster, Electron. Lett. **29,** 634 (1993); P. R. Tapster, J. G. Rarity, and P. C. M. Owens, Phys. Rev. Lett. **73,** 1923 (1994).
3. P. Hariharan, *Optical Interferometry* (Academic, San Diego, Calif., 1985).
4. 3×3 couplers have been used for the demodulation of orthogonal interferometer signals in fiber gyros [Ref. 7 and J. H. Ja, J. Mod. Opt. **42,** 117 (1995)] and some other sensor applications [R. Fuest, Tech. Messen **58,** 152 (1991); O. B. Wright, Opt. Lett. **16,** 56 (1991)].
5. K. Mattle, M. Michler, H. Weinfurter, A. Zeilinger, and M. Zukowski, Appl. Phys. B **60,** S111 (1995).
6. A. Zeilinger, M. Zukowski, M. A. Horne, H. J. Bernstein, and D. M. Greenberger, in *Proceedings of the Adriatico Workshop on Quantum Interferometry*, F. De Martini, G. Denardo, and A. Zeilinger, eds. (World Scientific, Singapore, 1993), p. 159; M. Reck and A. Zeilinger, in *Proceedings of the Adriatico Workshop on Quantum Interferometry*, F. De Martini, G. Denardo, and A. Zeilinger, eds. (World Scientific, Singapore, 1993), p. 170.
7. S. K. Sheem, J. Appl. Phys. **52,** 3865 (1981).
8. R. Ulrich, S. C. Rashleigh, and W. Eickhoff, Opt. Lett. **5,** 273 (1980).
9. R. M. A. Azzam and N. M. Bashara, *Ellipsometry and Polarized Light* (North-Holland, Amsterdam, 1977).